PAPER

The structure and interaction mechanism of a polyelectrolyte complex: a dissipative particle dynamics study†

Efrain Meneses-Juárez, César Márquez-Beltrán, Juan Francisco Rivas-Silva, Umapada Pal and Minerva González-Melchor*

The mechanism of complex formation of two oppositely charged linear polyelectrolytes dispersed in a solvent is investigated by using dissipative particle dynamics (DPD) simulation. In the polyelectrolyte solution, the size of the cationic polyelectrolyte remains constant while the size of the anionic chain increases. We analyze the influence of the anionic polyelectrolyte size and salt effect (ionic strength) on the conformational changes of the chains during complex formation. The behavior of the radial distribution function, the end-to-end distance and the radius of gyration of each polyelectrolyte is examined. These results showed that the effectiveness of complex formation is strongly influenced by the process of counterion release from the polyelectrolyte chains. The radius of gyration of the complex is estimated using the Fox–Flory equation for a wormlike polymer in a theta solvent. The addition of salts in the medium accelerates the complex formation process, affecting its radius of gyration. Depending on the ratio of chain lengths a compact complex or a loosely bound elongated structure can be formed.

1 Introduction

The attraction between molecules of different electric charge can be used to create colloidal complexes at the nanometer scale.[1–3] This is the case of polyelectrolyte complexes, materials formed with oppositely-charged macromolecules.[4–12] The self-assembly of these polyelectrolytes is relatively complicated and depends not only on the electrostatic interactions, but also on chain conformation of the polyelectrolytes and on counterion entropy variations. The development of polyelectrolyte complexes as biomaterials has theoretical and experimental interest because the complexation of proteins with polyelectrolytes is the basis of processes such as protein purification, enzyme immobilization, immunosensing, and the design of bioactive sensors.[13,14] Studies of polyelectrolyte complexes have also allowed to understand the behavior of some biological macromolecules, such as DNA-binding proteins;[15,16] in particular, Kabanov *et al.* have used DNA–polycation complexes for the delivery of genetic materials into cells, *i.e.*, for gene transfer and gene therapy.[17] The use of polymers in gene therapy systems is mainly motivated by their specific properties such as biodegradability,[18] biocompatibility,[19] and bioactivity.[20]

Instituto de Física "Luis Rivera Terrazas", Benemérita Universidad Autónoma de Puebla, Apartado Postal J-48, Puebla, 72570, Mexico.
E-mail: minerva@ifuap.buap.mx

† Electronic supplementary information (ESI) available. See DOI: 10.1039/c5sm00911a

In a full atomistic view, all atoms and molecules in the system can, in principle, be included in a molecular simulation. However it still has some limitations because the explicit inclusion of the solvent is the most time-consuming part in the calculations. In the last 15 years, mesoscale or coarse-grained computer simulations have emerged as important tools for studying the phenomenon described above; including applications to polymeric solutions, colloidal suspension, surfactants and biological membranes.[21–25] However, to increase the system size, some of these simulation schemes relax their treatments on the solvent particles. The absence of the solvent eliminates the hydrophobic effect that drives the formation, for example, of amphiphilic membranes or polymer aggregates. Therefore, it is necessary to include effective forces to restore solvent effects. An intermediate level between the atomistic view and the exclusion of the solvent is to incorporate the latter at some degree of resolution in the simulation. Indeed, coarse-grained simulations that include solvent particles, such as Dissipative Particle Dynamics (DPD), allow the simulation of very large systems in which hydrodynamic forces are taken into account, and their effects on soft matter can be better visualized.[26,27] In fact, DPD is a particle-based, explicit solvent simulation technique that was created for the simulation of fluids at larger lengths and time scales than that is possible using atomistic molecular dynamics, whilst retaining the hydrodynamic modes that are missing in techniques such as Monte Carlo and Brownian dynamics. DPD has also been reviewed and discussed as an useful thermostat in

studying equilibrium and non-equilibrium phenomena.[28] In the case of polyelectrolyte complexation, the electrostatic interaction plays a key role for understanding these phenomena. It has been found[29] that the formation of the complex depends on several factors such as chain size, charge distribution on the polyelectrolyte, ionic strength, pH, solvent type and thermal energy.

A very simplified model which serves as a reference system to study the complex formation is the ideal case of two single polyelectrolytes of opposite charge in solution. Previous simulation studies of two single polyelectrolytes were performed using Brownian dynamics simulations to explore the formation of their complex.[24,30] However, in those studies neither counterions nor salt were included explicitly. The complex formation has also been studied *via* Monte Carlo simulations in the absence of solvent, for instance Narambuena *et al.*[31] found different morphologies: toroids, rods and globular structures when an anionic chain and a cationic polymer are considered.

In the mesoscopic regime, the modeling of polyelectrolytes requires the calculation of the long-range electrostatic interactions at a mesoscopic level.[32] Groot[33] proposed their incorporation using an adapted version of the particle–particle particle–mesh (PPPM) method and charged distributions on DPD particles. With a similar spirit González-Melchor *et al.*[34] proposed a method where the Ewald[35] technique is combined with the idea of charge distribution on the DPD particles. One advantage of the latter is that all the tools developed for the Ewald technique, used in atomistic simulations, can be employed to improve the efficiency in the calculation of the reciprocal part by adopting approximate methods as the PPPM and particle mesh Ewald or by considering different charge distributions.[36,37]

Recently colloidal dispersions of polyelectrolyte complexes of sodium polystyrene sulfonate and polyallylamine hydrochloride have been prepared in aqueous solutions, finding that the effect of the ionic strength affects the size and stability of complex formation.[29]

The aim of this work is to investigate the interaction mechanism of a polyelectrolyte complex in terms of structural properties obtained from DPD simulations. We considered two oppositely charged chains of different sizes in water, under salt-free and salt-added conditions. The electrostatic interactions are calculated using the method proposed by González-Melchor *et al.*[34]

The rest of this paper is arranged as follows: Section 2 contains a brief description of the DPD method and the treatment of the electrostatics. In Section 3 we present the systems studied and the simulation details. Our results and discussion on structural properties are presented in Section 4. Conclusions are drawn in the final section.

2 The dissipative particle dynamics method

The DPD simulation method was introduced by Hoogerbrugge and Koelman[38] in 1992 for studying complex fluids with hydrodynamic phenomena. Later in 1995 it was modified by Español and Warren[39] to ensure a proper thermal equilibrium state of the system. The method was then applied by Groot and Rabone[40] to model biological membranes, where several atoms are united to a single particle. Since DPD preserves hydrodynamic modes, it is a very promising method for mesoscopic studies of soft matter. Recently the method has been applied for the studies of polymers,[41] microphase separation,[42] lipid bilayers[22,43,44] and other biological systems. The DPD method was originally proposed to study repulsive interactions. Later, it has been modified to include multibody effects, which allows the inclusion of attractive interactions to simulate vapor–liquid equilibrium.[45,46]

Although DPD simulation uses the integration principle of equations of motion, it takes into account the degrees of freedom of the smallest particles (functional groups or solvent), and hence larger systems can be sampled at a higher space-time scale at a coarse-grained level. In DPD, there are three types of forces between pairs of particles, they produce a rate of change in the linear momentum. A great advantage of the method is that it allows the use of longer time steps than those used in atomistic simulations, reducing the computation cost in the simulation time.

If we consider a particle i in the system interacting with its neighbors j, the total force acting on it can be written as $\mathbf{F}_i = \sum_{j \neq i} \left(\mathbf{F}_{ij}^C + \mathbf{F}_{ij}^D + \mathbf{F}_{ij}^R \right) + \sum_{j \neq i} \mathbf{F}_{ij}^S + \sum_{j \neq i} \mathbf{F}_{ij}^E$, where the term in parentheses is the force due to the interaction of neighboring particles. The superscripts C, D, and R mean conservative, dissipative, and random forces, respectively, while S corresponds to spring harmonic interaction between bonded monomers in the polyelectrolytes and E denotes the electrostatic force between charged pairs. This electrostatic contribution will be described below. The resultant force over all the systems is zero. The conservative part of the net force is given by $\mathbf{F}_{ij}^C = a_{ij}\omega^C(r_{ij})\hat{\mathbf{e}}_{ij}$, where $a_{ij} = a_{ji} > 0$, which indicates that this force is always repulsive, $r_{ij} = |\mathbf{r}_{ij}| = r$ is the distance between i-th and j-th particles and $\hat{\mathbf{e}}_{ij}$ is the unit vector along the relative position. DPD uses a function of simple linear weight; $\omega(r) = 1 - r/R_c$ for $r < R_c$ and $\omega(r) = 0$ for $r > R_c$, where R_c is the cut-off distance. The weights for the conservative, dissipative and random forces are related to $\omega(r)$ by $\omega(r) = \omega^C(r) = \sqrt{\omega^D(r)} = \omega^R(r)$. The dissipative force, $\mathbf{F}_{ij}^D$, is proportional to the velocity with which two particles approach each other. It is $\mathbf{F}_{ij}^D = -\gamma_{ij}\omega^D(r_{ij})[\hat{\mathbf{e}}_{ij}\cdot\boldsymbol{\nu}_{ij}]\hat{\mathbf{e}}_{ij}$, where $\gamma_{ij} = \gamma_{ji} > 0$ and $\boldsymbol{\nu}_{ij} = \boldsymbol{\nu}_i - \boldsymbol{\nu}_j$ is the difference of particle velocities. The term $\boldsymbol{\nu}_{ij}\cdot\hat{\mathbf{e}}_{ij}$ is positive if the particles are close, in this case the dissipative force is repulsive. If the particles are well apart, $\boldsymbol{\nu}_{ij}\cdot\hat{\mathbf{e}}_{ij}$ is negative and the dissipative force is attractive. The random force $\mathbf{F}_{ij}^R$ is $\mathbf{F}_{ij}^R = \sigma_{ij}\omega^R(r_{ij})\xi_{ij}\hat{\mathbf{e}}_{ij}$, where σ_{ij} determines the strength of the random force, ξ_{ij} is a random number which is uniformly distributed between 0 and 1 with Gaussian distribution, zero mean, and unit variance. The intramolecular interaction between monomers in a chain is given by harmonic forces, *i.e.*, they are bonded by $\mathbf{F}_{ij}^S = -K(r - r_0)\mathbf{r}_{ij}/r$, where K is the spring constant and r_0 is the equilibrium bond distance. They were chosen as $K = 4.0 \text{ N m}^{-1}$ in SI units and $r_0 = 0$ as in ref. 26. Under such a force field, the DPD particles move following Newton's equations of motion

$$\mathbf{F}_i = m_i \frac{\mathrm{d}\mathbf{v}_i}{\mathrm{d}t}. \tag{1}$$

We used a modified version of the velocity Verlet algorithm DPD-VV[47] to integrate the equations of motion. If $\sigma_{ij} = \sigma$, $\gamma_{ij} = \gamma$ and the dissipative and random forces are related through the fluctuation–dissipation (FD) theorem $\sigma^2 = 2\gamma k_B T$, an important implication is that the canonical distribution emerges naturally and $\mathbf{F}_{ij}^D$ and $\mathbf{F}_{ij}^R$ act as an in-built thermostat. In the FD relation, T is the absolute temperature and k_B is the Boltzmann's constant. In this standard DPD formalism, the conservative force is a soft repulsive term of short-range, which models the soft nature of the DPD particles.

We calculated electrostatic interactions in DPD by using the Ewald version previously proposed.[34] In this method, the main idea is to combine much of the knowledge developed for electrostatic interactions in atomistic simulations, with Groot's idea of assigning charge distributions on DPD particles.[33] In this way the Ewald simulation method can be applied to calculate the electrostatic interaction energy and the force between two charged particles in the system, being aware that in this meso-scopic description a charged particle carries a charge distribution, instead of a point charge. Since this Ewald approach was proposed, it has been successfully applied to describe polyelectrolyte brushes,[48] diblock copolymers,[49] electrolytes[50] and was also included in the DL_MESO simulation package.[51] We briefly outline the method, which is fully described in ref. 34.

In DPD methodology, we considered Slater-type distributions on charged DPD particles, given by

$$\rho(R) = \frac{q}{\pi\lambda^3}e^{-2R/\lambda},\qquad(2)$$

where λ is the decay length of the distribution, R is the radial distance measured from the center of the particle and q is the total charge on the particle. For the distribution given in eqn (2) the energy and the force between two charged particles separated by a distance $r = r_{ij}$ are given by[52]

$$u_{ij}(r) = \frac{1}{4\pi\varepsilon_0\varepsilon_r}\frac{q_i q_j}{r}\left[1 - (1 + \beta r)e^{-2\beta r}\right],\qquad(3)$$

$$\mathbf{F}_{ij}^E = \frac{1}{4\pi\varepsilon_0\varepsilon_r}\frac{q_i q_j}{r^2}\left\{1 - e^{-2\beta r}[1 + 2\beta r(1 + \beta r)]\right\}\hat{r},\qquad(4)$$

where $\beta = 1/\lambda$, ε_0 and ε_r are the dielectric constants of vacuum and water at room temperature, respectively. The first term in these equations is the long-range $1/r$ contribution, which is calculated by using the Ewald expression given below in eqn (5).

In the Ewald summation method, the total electrostatic energy for a periodic system of N point charges with positions $\mathbf{r}_1, \mathbf{r}_2,...,\mathbf{r}_N \equiv \mathbf{r}^N$ is written as[34,53]

$$
\begin{aligned}
U(\mathbf{r}^N) &= \frac{1}{4\pi\varepsilon_0\varepsilon_r}\left[\sum_i \sum_{j>i} q_i q_j \frac{\mathrm{erfc}(\alpha r)}{r} + \frac{2\pi}{V}\sum_{k\neq 0}^{\infty} Q(\mathbf{k})S(\mathbf{k})S(-\mathbf{k})\right.\\
&\left. - \frac{\alpha}{\sqrt{\pi}}\sum_i^N q_i^2\right],
\end{aligned}
\qquad(5)
$$

where q_i is the charge of particle i, $V = L^3$ is the volume of the cubic simulation cell of length L and erfc(x) is the complementary

error function. The terms in the right-hand side of eqn (5) are the real, the reciprocal and the self-energy contributions, $\mathbf{k}$ is the reciprocal vector $\mathbf{k} = 2\pi(m_x, m_y, m_z)/L$, where m_x, m_y, m_z are integer numbers. The parameter α controls the range of the real space contribution. The quantities $Q(\mathbf{k})$ and $S(\mathbf{k})$ are defined as

$$Q(\mathbf{k}) = \frac{e^{-k^2/4\alpha^2}}{k^2},\quad S(\mathbf{k}) = \sum_{i=1}^N q_i e^{i\mathbf{k}\cdot\mathbf{r}},\qquad(6)$$

where k is the magnitude of $\mathbf{k}$. eqn (5) produces the exact $1/r$ dependence in systems of point charges, capturing the long-range nature of electrostatic interactions for point charges.

Going back to the treatment of electrostatics in DPD, we calculated the $1/r$ and $1/r^2$ terms in eqn (3) and (4) as is commonly done in atomistic simulations, keeping in mind that in the DPD description, this is just a part of the electrostatic interaction. The full electrostatic pair potential and the electrostatic force between two DPD charged particles are then given by eqn (3) and (4), respectively, where the latter terms in these equations account for the energy and the force due to the continuous part of the charge distributions, which of course, are included in the DPD code.

Since the electrostatic force is conservative, the sum of $\mathbf{F}_{ij}^E$ contained in eqn (4) and the original conservative part $\mathbf{F}_{ij}^C$ determine the thermodynamic behavior of the system.

3 Systems and simulation details

In this work we will keep the same values for the parameters a_{ij}'s in the conservative force, allowing the electrostatics to play the main role in complex formation.

In order to study the effect of chain size on the structure of the complex, we considered two different cases: salt-free systems and systems with monovalent salt (Na^+ and Cl^- ions), added in concentrations of 0.1 M, 0.3 M,..., 0.9 M. In both the salt-free and salt-added cases, we considered that the anionic chain increases in size from 10% to 100% with respect to the cationic chain. The number of monomers in the cationic polyelectrolyte is kept constant with 100 DPD particles in all the simulations maintaining a charge fraction constant, equal to 1 (fully charged). To preserve charge neutrality in the systems, 100 counterions of net charge $-e$ were added to compensate the cationic chain charge, and the required counterions of net charge $+e$ were added for the anionic chain, which was also fully charged.

The simulations were performed under canonical conditions of N, V, and T constants. We used R_c, $k_B T$ and the mass of a DPD particle, m, as units of length, energy and mass, respectively. The temperature was kept constant at 298 K for all the simulations. The interaction parameter for the conservative, dissipative and random forces was $a_{ij} = 78.33$ for all pairs ij, which reproduces the compressibility of pure water at room temperature;[54] $\gamma_{ij} = 4.5$, and $\sigma_{ij} = 3.0$ lead to a reduced temperature $T^* = T/T_0 = 1$ with $T_0 = 298$ K. For the electrostatic contribution, we used the values previously employed.[34] Ewald real forces were truncated at $R_c^{real} = 3.0R_c$, where $R_c = 270(\mathring{A})^{1/3} = 6.46333$ Å and $\alpha = 0.15$ Å^{-1}. For the reciprocal part, we calculated

the summation to a maximum number vector $\mathbf{k}_{max}$, defined by $(m_x, m_y, m_z)^{max} = (5,5,5)$. With these parameters, the dimensionless Ewald errors in the energy were $\left[\text{erfc}\left(\alpha R_c^{real*}\right)/R_c^{*real}\right] \sim 10^{-5}$ for the real part and $\left[\exp\left(-k_{max}^{*2}/4\alpha^{*2}\right)/k_{max}^{*2}\right] \sim 10^{-3}$ for the reciprocal contribution. This choice of Ewald parameters was done to keep these values as a reference set. A more detailed analysis is needed to explore the effect of different choices, not just for the Ewald part, but also for the parameter $1/\lambda$ controlling the decay of the charge distribution or the charge distribution itself. In this sense, the recent study performed by Warren and Vlasov is valuable.[55] The Slater distribution assigned on charged particles was used with the value of $\beta^* = \beta R_c = R_c/\lambda = 0.929$.[34] The reduced time step used to integrate the equations of motion was $\Delta t^* = \Delta t(k_B T/m R_c^2)^{1/2} = 0.02$.

Once the equilibrium was reached, we obtained the properties making an average over at least 4×10^5 time steps after 1×10^5 equilibrium iterations. The estimated Δt value in real unit is 0.066×10^{-12} s, and the estimated simulation time is $t_{sim} \sim 26$ ns.

The total particles were allocated into a cubic cell with reduced volume, $V^* = 15 \times 15 \times 15$. The density of the system was always $\rho^* = N/V^* = 3$. The salt concentration in the systems was calculated using[34] $c^{real} = (N_{NaCl}/V^*)/(R_c^3 N_A)$, where N_{NaCl} is the number of salt molecules and N_A is the Avogadro number. Hereafter we will denote the cationic chain as PAH$^+$ and the anionic polymer as PSS$^-$ in order to distinguish them, and their counterions will be denoted Cl$^-$ and Na$^+$, respectively. The monovalent salt is sodium chlorine, represented as additional Cl$_{salt}^-$ and Na$_{salt}^+$ ions, which change in number depending on the salt concentration. Finite size effects on the calculated properties were studied and are presented in the ESI.†

4 Results and discussion

4.1 Radial distribution functions

The structure of solvent and ions were determined by calculating the radial distribution functions (RDFs). All lengths will be given in reduced units. In the case of salt-free aqueous solution containing two oppositely charged polyelectrolytes of different sizes, the results of RDFs for the cationic polyelectrolyte–solvent pair, $g(r)_{PAH^+/Solv}$, are shown in Fig. 1 for five different chain length ratios of PSS$^-$ with respect to the PAH$^+$ chain, defined as $\delta = $ (number of monomers in the PSS$^-$/number of monomers in the PAH$^+$) $\times$ 100%.

As can be observed, there is no artificial pair formation at $r^* = 0.0$. On increasing the distance r^*, $g(r)_{PAH^+/Solv}$ shows a pattern of peaks and troughs attenuating until reaching a constant value, which is the typical characteristic of liquid structures.[56] When the anionic chain length increases, $g(r)_{PAH^+/Solv}$ decreases in intensity, but the solvent–solvent structure remains unaltered (not shown). This effect is due to the fact that our simulations include about 10 000 DPD water particles while the cationic and anionic chains together contain a maximum of 200 particles, i.e., the polyelectrolyte concentration is 1–2% of the total number of particles. The reduction of $g(r)_{PAH^+/Solv}$ on the increase of anionic chain can
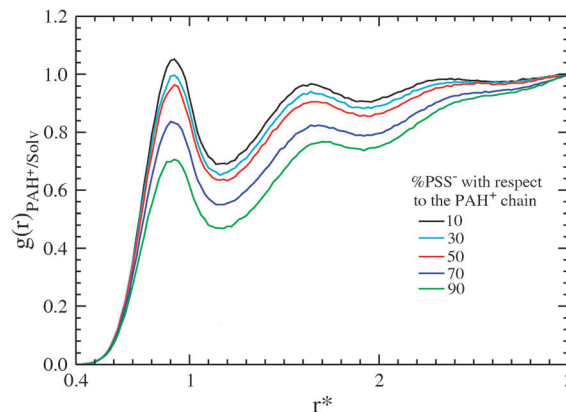

Fig. 1 Pair correlation function between the cationic polyelectrolyte and the solvent ($g(r)_{PAH^+/Solv}$) as a function of the anionic chain variation for salt-free systems.

be due to a small displacement of the water particles at the moment of complex formation. Indeed, this explanation is justified because the $g(r)_{PAH^+/Solv}$ peak is related to the maximum probability of finding the cationic polyelectrolyte–solvent pair.

We also analyzed the pair correlation function for the cationic polyelectrolyte and their counterion $g(r)_{PAH^+/Cl^-}$, as shown in Fig. 2. The decrease of $g(r)$ is more pronounced than the pair correlation function of the cationic polyelectrolyte–solvent. However, the variation of $g(r)$ is not oscillatory. Rather it has a peak at around $r^* \approx 0.9$, and decays rapidly until $r^* \approx 1.2$. After this r^*, $g(r)$ decays slowly. This peak suggests again that the probability of finding this particle pair at distances longer than 1.2 is low, indicating that the counterion and the cation remain close to each other. The position of the pair correlation function maximum (Fig. 2) has a physical meaning related to the Bjerrum length, $l_B = 0.7$ nm at $T = 298$ K,[57] while the decrease of $g(r)_{PAH^+/Cl^-}$ is related to the behaviour of the pair correlation function of the cationic–anionic polyelectrolytes (Fig. 3).

As can be seen from Fig. 3, the magnitude of the function $g(r)_{PAH^+/PSS^-}$ is very high, and is even higher when the anionic chain size increases, making the probability of finding the anionic–cationic chains together higher. The behavior is opposite to that of the pair correlation between the cationic polyelectrolyte and its counterion, suggesting that the counterions are released when the length of the anionic chain increases, giving rise to the formation of the polyelectrolyte complex.

The obtained results are in good agreement with earlier theoretical predictions, demonstrating that the driving force for the overall complexation process is not determined only by the electrostatic interactions, but also by the process of low-molecular-weight counterion release, i.e., a favorable entropy change in the counterions.[4,6,58,59] Now we will compare the results of $g(r)$ previously discussed with the calculated $g(r)$ when an ionic strength is applied in the system, i.e., with the addition of monovalent salt.

In Fig. 4 we present the behavior of $g(r)_{PAH^+/Cl^-}$. As we mentioned earlier, $g(r)_{PAH^+/Cl^-}$ decreases when the anionic chain length increases, which is related to the release of their counterions.

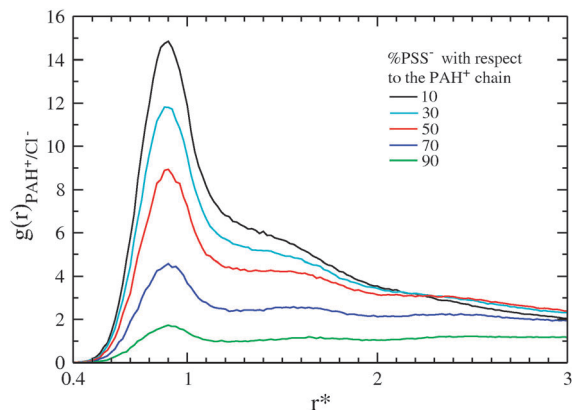Fig. 2 Pair correlation function between the cationic polyelectrolyte and its counterion ($g(r)_{PAH^+/Cl^-}$) as a function of anionic chain variation for salt-free systems.
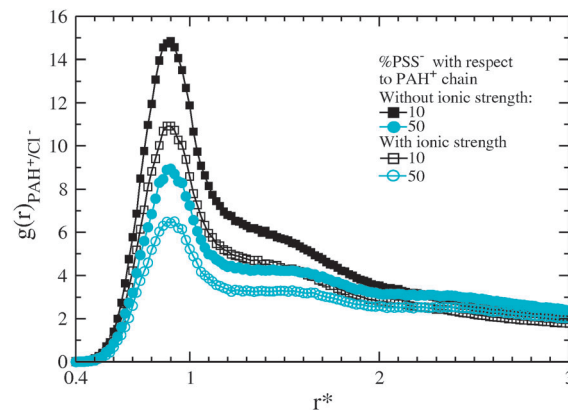

Fig. 4 Pair correlation function of the cationic polyelectrolyte and its counterion ($g(r)_{PAH^+/Cl^-}$) for salt-free systems (filled symbols) and systems with salt added (open symbols) when the anionic chain (PSS$^-$) increases from 10% to 50% in size with respect to the cationic chain (PAH$^+$).
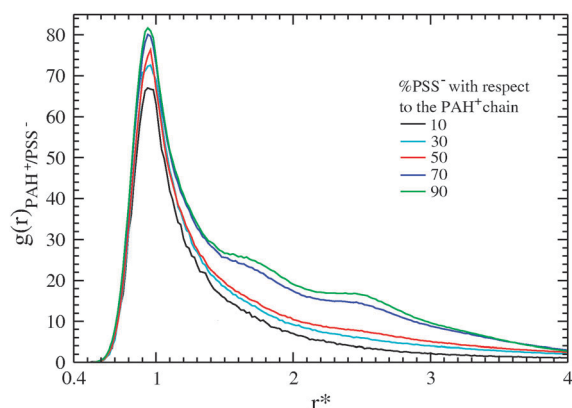

Fig. 3 Pair correlation function between the cationic and anionic polyelectrolytes ($g(r)_{PAH^+/PSS^-}$) in the salt-free system as a function of anionic chain length.
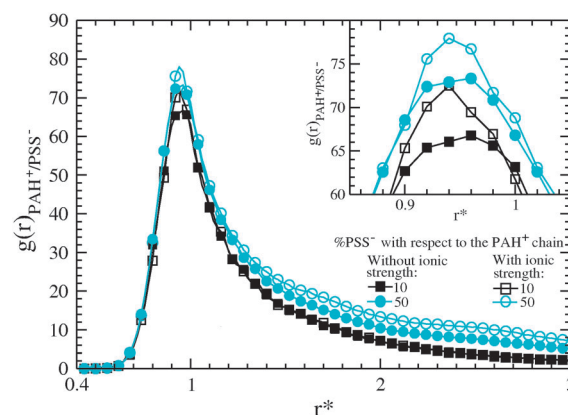

Fig. 5 Comparison of the pair correlation function between cationic and anionic polyelectrolytes ($g(r)_{PAH^+/PSS^-}$) for salt-free and salt added systems when the anionic chain increases from 10% to 50% in size with respect to the cationic chain.

However, when a monovalent salt is added to the system, the intensity of the maximum of $g(r)_{PAH^+/Cl^-}$ function is much lower than in the salt-free case. The influence of salt is also observed on $g(r)_{PAH^+/PSS^-}$ of a cationic–anionic polyelectrolyte pair, where the intensity of the maximum is also high with respect to $g(r)_{PAH^+/PSS^-}$ of the salt-free system (Fig. 5). This behavior can be associated with the screening phenomenon produced by low-molecular-weight ions, since the pair correlation between cation–counterion decreases on incorporating ionic strength (incorporating ions in the system). On the other hand, the nature of complexation between the ionic chains for the two cases (with or without salt) is also influenced by the nature of the bonds between the monomers (in this case harmonic forces). However, inclusion of salt in the system could lead to many different chain conformations before of the occurrence of complexation. It has been found that, while a neutral linear polymer chain in a good polar solvent (where the number of polymer–solvent contacts are maximized) is usually found in a random conformation in solution (closely approximating a self-avoiding three-dimensional random walk), the charges in linear polyelectrolyte chains will repel each other (Coulomb repulsion),

forcing the polymer chains to adopt a more expanded conformation in solution. For a high concentration of salt in the solution, the charges will be screened, and consequently, the polyelectrolyte collapses to a more conventional conformation (essentially identical to a neutral chain in good solvent).[60] Thus, the structure of the polyelectrolyte complex can be understood from the polyelectrolyte conformations formed on adding the salt into the system. Indeed, a systematic study on the different conformations adopted by the chains has to be performed during complex formation. In order to obtain information on complex conformation, we have studied the end-to-end distance and the radius of gyration of each polyelectrolyte, when the anionic chain increases in size in the salt-free and salt-added cases.

4.2 Radius of gyration and the end-to-end distance

The radius of gyration R_g is an important parameter for the description of the conformation of polyelectrolytes. The magnitude of R_g provides an idea of chain size. The size and shape of a single polyelectrolyte chain depend strongly on the electrostatic

interaction between its monomers, solvent type, ionic strength and temperature. In our system, as a natural consequence of the Coulombic interaction, two chains of opposite charge attract one another forming the complex. In Fig. 6 we calculated $\langle R_g \rangle$, where $\langle \ldots \rangle$ means average over time for each polyelectrolyte and its variation as a function of the ratio δ. Statistical errors in the average values of radius of gyration and end-to-end distance were about 10% and 20%, respectively. They are displayed in Fig. 6.

Fig. 6(a) shows the variation of $\langle R_g \rangle$ of the PAH$^+$ and PSS$^-$ chains for the salt-free case. As we can see, magnitudes $\langle R_g \rangle$ depend on the number of charged sites on the PSS$^-$ chain. The radius of gyration of PAH$^+$ decreases while that of PSS$^-$ increases up to about $\delta = 40\%$; after this value, both chains have approximately the same $\langle R_g \rangle$. The results of $\langle R_g \rangle$ for 0.1 M concentration of salt are shown in Fig. 6(b). Similar to the salt-free case, we observed a linear increase of $\langle R_g \rangle$ for PSS$^-$; moreover its size is remarkably similar to that of PAH$^+$ for $\delta \geq 50\%$. Nevertheless, for the cationic polyelectrolyte, its radius of gyration decreases slightly. Although a similar behavior was observed for higher salt concentrations (not shown), the values of R_g for PAH$^+$ and PSS$^-$ decreased approximately 30% in comparison with the salt-free case, regardless of the PSS$^-$/PAH$^+$ ratio. As the polyelectrolytes used in this study are flexible, they can adopt a great number of conformations depending on the medium. The distance between the first and the last link, called the end-to-end distance R_{ee}, is also a useful parameter for characterizing representative polyelectrolyte extension.

The variation of $\langle R_{ee} \rangle$ for the anionic and cationic polyelectrolytes with the variation of anionic chain size for the salt-free case is shown in Fig. 6(c). For the PSS$^-$ chain, the magnitude of $\langle R_{ee} \rangle$ increases linearly until $\delta = 40\%$, and then decreases. Nevertheless, for PAH$^+$ the magnitude of $\langle R_{ee} \rangle$ decreases with the increase of δ. Such behaviors of R_g and R_{ee} are due to an increase in number of charged monomers and consequently, the release of their counterions encourage the PAH$^+$ polymer to fold onto the PSS$^-$ chain in a structure as in a zipper. It can be understood as a high cooperativity between both chains to form the complex.
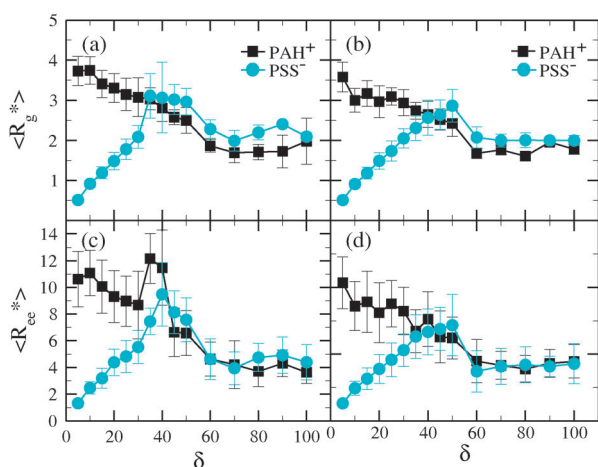

Fig. 6 Dependence of the radius of gyration R_g, and end-to-end distance R_{ee}, with the anionic chain size PSS$^-$ for systems: (a) and (c) without ionic strength; (b) and (d) with salt at 0.1 M concentration.

Finally, the behavior of $\langle R_{ee} \rangle$ for the salt-added system with 0.1 M concentration is presented in Fig. 6(d). The results are similar to those of the salt-free case. For this system, both polyelectrolytes exhibit a similar $\langle R_{ee} \rangle$ for values $\delta \geq 50\%$. In addition, for ratios less than $\delta = 50\%$, the end-to-end distance takes lower values for both polyelectrolytes. Moreover, the maximum $\langle R_{ee} \rangle$ observed for PAH$^+$ in the salt-free case is absent.

The effect of salt concentration on the complex formation process has been studied further, and is presented in the following section.

4.3 Radius of gyration of the complex

In an attempt to obtain an estimation for the radius of gyration of the complex $R_{g\text{-}Complex}$, in terms of the radius of gyration of the individual polyelectrolyte chains of opposite charges, R_g^+ and R_g^-, we consider an approximation based on the result obtained by Meng et al.,[61] where they related the hydrodynamic radius with the radius of gyration for one polymer chain in solution. We make the assumption that once the complex is formed, the polyelectrolyte chains behave as a wormlike polymer in a theta solvent.[62] Following these ideas, we propose that the radius of gyration of the complex can be obtained to a first approximation by using the Fox–Flory relation,[63] which we rewrite in our case as

$$R_{g\text{-}Complex}{}^3 = \frac{M_{Complex}[\eta]_{Complex}}{\phi^{Complex}} \quad (7)$$

where $M_{Complex}$ is the molecular weight of the polymer complex, $[\eta]_{Complex}$ is the intrinsic viscosity and $\phi^{Complex}$ is a Flory's parameter associated with the complex and solvent. In eqn (7), $[\eta]_{Complex} = k_{Complex}M_{Complex}^a$ is the analogue of the Mark–Houwink equation. Here $k_{Complex}$ and a are the Mark–Houwink parameters, which depend on the specific polymer, the solvent and the temperature.[61] Applying eqn (7) with $M_{Complex} = M^+ + M^-$, where M^+ and M^- are molecular weights of the polycation and polyanion, respectively, we have

$$R_{g\text{-}Complex}{}^3 = \frac{M^+\left[\eta_{Complex}\right]}{\phi_{Complex}} + \frac{M^-\left[\eta_{Complex}\right]}{\phi_{Complex}}. \quad (8)$$

In our simulations, the relation between the molecular weight of polycation with respect to the polyanion is $M^- = \zeta M^+$, where ζ is a factor that relates the size of the polyelectrolyte chains (values between 0 and 1). The intrinsic viscosity can be rewritten as

$$[\eta_{Complex}] = k_{Complex}M_{Complex}^a = k_{Complex}(M^+)^a (1 + \zeta)^a. \quad (9)$$

Using both the Fox–Flory equation $(R_g^+)^3 = [\eta^+]M^+/\phi^+$ and the Mark–Houwink relation $[\eta^+] = k^+(M^+)^a$ for the cationic polyelectrolyte and replacing eqn (9) into eqn (8), and considering theta solvent conditions $a = 1/2$ (see ref. 62), we write the radius of gyration of the complex as

$$R_{g\text{-}Complex}{}^3 = \frac{k_{Complex}\phi^+}{k^+\phi^{Complex}}\left(R_g^+\right)^3 [1 + \zeta]^{3/2}, \quad (10)$$

where R_g^+ is the radius of gyration of the polycation and ϕ^+ is the Flory's parameter of the polycation. In this work we take $\phi^{\text{Complex}} \approx \phi^+$ and $k_{\text{Complex}} \approx k^+$, under the assumption that the polycation and the complex have approximately the same solvent-interaction under very diluted conditions. Finally, we can write

$$R_{\text{g-Complex}} = R_g^+ (1 + \zeta)^{1/2}. \quad (11)$$

This equation describes the change in the radius of gyration of the complex with respect to the behavior of the radius of gyration of the polycation when the anionic chain increases. The values of $R_{\text{g-Complex}}$ obtained using eqn (11) as a function of δ for different concentrations of NaCl are shown in Fig. 7. The decay of $R_{\text{g-Complex}}$, when δ increases, is related to the conformation of the individual polyelectrolyte chains, Fig. 6(b) and (d). The cationic polyelectrolyte strongly influences the behavior of the complex, as can be seen from eqn (11), where the values of R_g^+ obtained from the simulations decrease more rapidly than the factor containing the growth of the anionic chain, $(1 + \zeta)^{1/2}$.

As can be observed, for 0.1 M of NaCl, a drastic conformational change occurs at about $\delta = 60\%$. This behavior of $R_{\text{g-Complex}}$ obtained in our study suggests that at low ionic concentration (0.1 M), the presence of Na and Cl ions causes that the electrostatic persistence length of each polyelectrolyte decreases, giving rise to more flexible chains. When the value of δ is close and higher than 60% the number of released counterions increases, giving rise to more compact structures of the complex (see snapshots in Fig. 7).

However, for higher concentrations of NaCl a smooth change in $R_{\text{g-Complex}}$ was observed, although some reminiscent of the drastic conformational change can still be appreciated for 0.7 M and 0.9 M concentrations at about $\delta = 60\%$. The increase in salt concentration in the solution produces a deswelling of

the complex, leading to a smooth conformational transition when δ increases. A similar phenomenon has been observed by Dautzenberg et al.[64,65] for a mixture of two oppositely charged polyelectrolytes in aqueous solution. They found that a very small amount of sodium chloride added to the solution leads to a drastic decrease of aggregation (deswelling of the polyelectrolyte complex), while higher ionic strength results in macroscopic flocculation.

Our results state that as we increased both the salt concentration in the system and the size of the PSS⁻ chain, a crossover from an extended to a compact polyelectrolyte complex occurs. This behavior could be related to a phase change (for instance, from liquid to gel) although additional work is required to address this issue.

4.4 Energy and entropy of the complex

We analyzed the energy and the entropy of the systems to describe the structure and interaction mechanism of complex formation. The internal energy of the system was calculated as the sum of the kinetic, conservative, bonding, and electrostatic contributions. More details on the energy calculations are given in the ESI.† Particularly, the electrostatic energy U_{electr} was obtained for $\delta = 10$, 40, and 80% under salt-free and salt-added (0.1 M) conditions.

We note that upon increasing the chain size of the anionic polyelectrolyte from $\delta = 10\%$ to $\delta = 80\%$, $U_{\text{electr}}/k_B T_0$ decreases from 102.5 to about 91.5 for the salt-free case, as shown in Fig. 8. A similar behavior is found for a salt concentration of 0.1 M (not shown). The effect is associated to the shape of the complex, as can be observed in the snapshots presented in Fig. 7, where the complex changes from an extended to a compact structure.

The entropy of the system can be determined using the relation proposed in ref. 24, eqn (3.6). In our case, we consider the relationships $N_{-,p} = \zeta N_{+,p}$ and $\phi_{-,p} = \zeta \phi_{+,p}$, where $N_{-,p}$ and $N_{+,p}$ are the number of monomers in the anionic and cationic chains, respectively, ζ is a factor that relates the size of the polyelectrolytes, previously defined in Section 4.3. $\phi_{+,p}$ is the volume fraction of the cationic chain and $\phi_{+,c}$ the volume fraction of its counterions. Following a similar derivation for the change in entropy, before and after complex formation,[24] we obtained

$$\Delta S = -k_B \left[N_\pm \ln \frac{(1 + \zeta)}{\phi_{+,p}^\zeta} + \ln \left[\phi_{+,c} \right]^{N_{+,c}(1+\zeta)} \right], \quad (12)$$

where $N_\pm$ is the number of complexes in the system, in our case $N_\pm = 1$. The first term in eqn (12) is the entropy of the chain folding and the second term is the counterion release entropy. The second term dominates over the first when the anionic size increases (ζ), i.e., counterion release entropy contributes more to the complexation.

The change in entropy depends on the growth of the anionic chain through the parameter ζ. Applying this equation to $\delta = 10$, 40 and 80%, it is observed that the entropy increases, while the electrostatic energy decreases, Fig. 8. These results are consistent with the radial distribution functions obtained from the simulation for the polycation–counterion pair, $g(r)_{\text{PAH}^+/\text{Cl}^-}$,
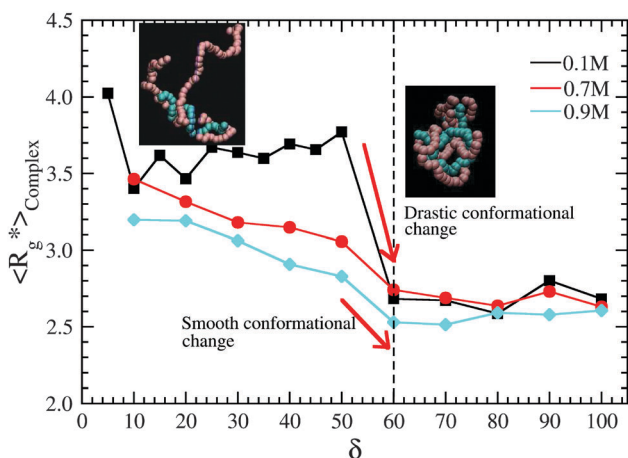

Fig. 7 Radius of gyration of the complex as a function of PSS⁻ size and ionic strength of the solution. The vertical dashed line indicates the ratio at which a change from an extended to a compact complex structure appears for the systems with 0.1 M of NaCl. Arrows indicate the regions of crossover from a drastic to a smooth conformational change. The insets on left and right show the polyelectrolyte complex for $\delta = 30\%$ and 60%, respectively, at 0.1 M NaCl concentration.
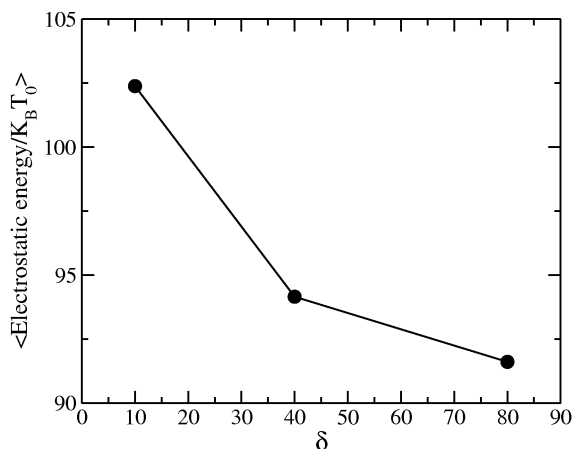
Fig. 8 Electrostatic energy for different values of δ for the salt-free case.

observed in Fig. 2. In fact, on increasing the size of the anionic chain, the probability of finding the polycation–counterion pair decreases due to increased release of counterions.

5 Conclusions

Structural properties of cationic PAH^+ and anionic PSS^- polyelectrolytes and their complex formation behaviors in salt-free and salt-added aqueous solution were studied through dissipative particle dynamics simulations for different concentrations of PSS^-. The behavior of radial distribution functions for the salt-free case suggests an expulsion of counterions that favors the formation of the complex, *i.e.*, PAH^+ and PSS^- are very cooperative. The variation of the radius of gyration shows that for concentrations (δ) less than 40%, R_g^+ is larger than R_g^- and the average conformation of PAH^+ is weakly affected in the presence of PSS^-, leading to the formation of extended aggregates. For $\delta > 60\%$, the radius of gyration R_g^+ reduces drastically, giving raise to the formation of compact aggregates.

For salt containing systems, the ionic strength modifies the configuration of PAH^+ and PSS^- chains. The presence of salt in the system enhances the formation of the polyelectrolyte complex. The radius of gyration R_g^- of PSS^- increases linearly as a function of the number of monomers along the chain for $\delta < 40\%$. In the $40\% < \delta < 60\%$ range, the radius of gyration decreases until it reaches a constant value. On the other hand, R_g^+ decreases gradually attaining a constant value for ratios higher than 60%.

The variations of radius of gyration of the complex suggest that the polyelectrolytes form two kinds of structures: extended and compact complexes. The former corresponds to high values of $R_{g\text{-Complex}}$, which occurs for length ratios $\delta \leq 60\%$, and the latter (smaller $R_{g\text{-Complex}}$ values) corresponds to length ratios $\delta \geq 60\%$. For lower salt concentrations (~ 0.1 M) in the system, a drastic conformational change occurs when the size of the anionic chain increases. On the other hand, for higher concentrations of NaCl (0.7 to 0.9 M), a smooth conformational change in $R_{g\text{-Complex}}$ occurs, although some reminiscent of the earlier drastic change can still be appreciated for 0.7 M and

0.9 M at about $\delta = 60\%$. The results indicate that high salt concentration in the system produces a deswelling of the polyelectrolyte complex.

References

1 A. I. Petrov, A. Antipov and G. Sukhorukov, *Macromolecules*, 2003, **36**, 10079.
2 C. Schatz, A. Domard, C. Viton, C. Pichot and T. Delair, *Biomacromolecules*, 2004, **5**, 1882.
3 Y. Lvov, G. Decher and H. Moehwald, *Langmuir*, 1993, **9**, 481.
4 E. Tuchida and K. Abe, *Adv. Polym. Sci.*, 1982, **45**, 1.
5 V. A. Kabanov and A. V. Zezin, *Sov. Sci. Rev., Sect. B*, 1982, **4**, 207.
6 B. Philipp, H. Dautzenberg, K. J. Linow, J. Kötz and W. Dawydoff, *Prog. Polym. Sci.*, 1989, **14**, 91.
7 H. Dautzenberg and N. Karibyants, *Macromol. Chem. Phys.*, 1999, **200**, 188.
8 S. Dragan and M. Cristea, *Polymer*, 2002, **43**, 55.
9 G. Petzold and K. Lunkwitz, *Colloids Surf., A*, 1995, **98**, 225.
10 A. V. Kabanov, T. K. Bronich, V. A. Kabanov, K. Yu and A. Eisenberg, *Macromolecules*, 1996, **29**, 6797.
11 N. Acar, M. B. Huglin and T. Tulun, *Polymer*, 1999, **40**, 6429.
12 V. A. Izumrudov and B. Bunsenges, *J. Phys. Chem.*, 1996, **100**, 1017.
13 W. Ouyang and M. Müller, *Macromol. Biosci.*, 2006, **6**, 929.
14 V. Boeris, B. Farruggia, B. Nerli, D. Romanini and G. Picó, *Int. J. Biol. Macromol.*, 2007, **41**, 286.
15 S. Ahmad, M. M. Gromiha and A. Sarai, *Bioinformatics*, 2004, **20**, 477.
16 R. E. Langlois, M. B. Carson, N. Bhardwaj and H. Lu, *Ann. Biomed. Eng.*, 2007, **35**, 1043.
17 A. V. Kabanov, S. V. Vinogradov, Y. G. Suzdaltseva and V. Y. Alakhov, *Bioconjugate Chem.*, 1995, **6**, 639.
18 Y. L. Kuen, S. H. Wan and H. P. Won, *Biomaterials*, 1995, **16**, 1211.
19 S. Hirano, H. Seino, Y. Akiyama and I. Nonaka, *Polym. Eng. Sci.*, 1989, **59**, 897.
20 A. Domard and M. Domard, in *Polymeric biomaterials*, ed. S. Dimitru, M. Dekker Press, New York, 2011.
21 C. Brender and M. Danino, *J. Phys. Chem. B*, 1996, **100**, 17563.
22 T. Murtola, E. Falck, M. Patra, M. Karttunen and I. Vattulainen, *J. Chem. Phys.*, 2004, **121**, 9156.
23 J. C. Shillcock and R. Lipowsky, *Nat. Mater.*, 2005, **4**, 225.
24 Z. Y. Ou and M. Muthukumar, *J. Chem. Phys.*, 2006, **124**, 154902.

25 J. N. Israelachvili, *Intermolecular and Surface Forces*, Academic Press, 3rd edn, 2011.

26 R. D. Groot, *Langmuir*, 2000, **16**, 7493.

27 J. C. Shillcock, *Computer Simulation*, ed. A. Zvelindovsky, Springer, 2007, 1st edn, Part III, p. 529.

28 T. Soddemann, B. Dunweg and K. Kremer, *Phys. Rev. E: Stat., Nonlinear, Soft Matter Phys.*, 2003, **68**, 046702.

29 C. Márquez-Beltrán, L. Castañeda, M. Enciso-Aguilar, G. Paredes-Quijada, H. Acuña-Campa, A. Maldonado-Arce and J. F. Argillier, *Colloid Polym. Sci.*, 2013, **291**, 683.

30 M. A. Trejo-Ramos, F. Tristán, J. L. Menchaca, E. Pérez and M. Chávez-Paez, *J. Chem. Phys.*, 2007, **126**, 014901.

31 C. F. Narambuena, E. P. M. Leiva, M. Chávez-Paez and E. Pérez, *Polymer*, 2010, **51**, 3293.

32 G. A. Cisneros, M. Karttunen, P. Ren and C. Sagui, *Chem. Rev.*, 2014, **114**, 779.

33 R. D. Groot, *J. Chem. Phys.*, 2003, **118**, 11265.

34 M. González-Melchor, E. Mayoral, E. Velázquez and J. Alejandre, *J. Chem. Phys.*, 2006, **125**, 224107.

35 P. Ewald, *Ann. Phys.*, 1921, **64**, 253.

36 P. T. Kiss, M. Sega and A. Baranyai, *J. Chem. Theory Comput.*, 2014, **10**, 5513.

37 G. A. Cisneros, J. P. Piquemal and T. A. Darden, *J. Chem. Phys.*, 2006, **125**, 184101.

38 P. J. Hoogerbrugge and J. M. V. A. Koelman, *Europhys. Lett.*, 1992, **19**, 155.

39 P. Español and P. B. Warren, *Europhys. Lett.*, 1995, **30**, 191.

40 R. D. Groot and K. L. Rabone, *Biophys. J.*, 2001, **81**, 725.

41 P. B. Warren, *Curr. Opin. Colloid Interface Sci.*, 1998, **3**, 620.

42 R. D. Groot, T. J. Madden and D. J. Tildesley, *J. Chem. Phys.*, 1999, **110**, 9739.

43 M. Venturoli and B. Smit, *Phys. Chem. Comm.*, 1999, **10**, 45.

44 R. D. Groot, *Langmuir*, 2003, **16**, 7493.

45 S. Y. Trofimov, E. L. F. Nies and M. A. J. Michels, *J. Chem. Phys.*, 2002, **117**, 9383.

46 I. Pagonabarraga and D. Frenkel, *J. Chem. Phys.*, 2001, **115**, 5015.

47 I. Vattulainen, M. Karttunen, G. Besold and J. M. Olson, *J. Chem. Phys.*, 2002, **116**, 3967.

48 C. Ibergay, P. Malfreyt and D. J. Tildesley, *Soft Matter*, 2011, **7**, 4900.

49 Z. Posel, Z. Limpouchova, S. K. Sindelka, M. Lisal and K. Prochazka, *Macromolecules*, 2014, **47**, 2503.

50 A. Ghoufi and P. Malfrey, *J. Chem. Theory Comput.*, 2012, **8**, 787.

51 M. A. Seaton, R. L. Anderson, S. Metz and W. Smith, *Mol. Simul.*, 2013, **39**, 796.

52 M. Carrillo-Tripp, *Selectividad Iónica de Canales Biológicos*, PhD thesis, Universidad Autónoma del Estado de Morelos, México, 2005.

53 P. P. Ewald, *Ann. Phys.*, 1921, **64**, 253.

54 R. D. Groot and P. Warren, *J. Chem. Phys.*, 1997, **107**, 4423.

55 P. B. Warren and A. Vlasov, *J. Chem. Phys.*, 2014, **140**, 084904.

56 J. P. Hansen and I. R. McDonald, *Theory of Simple Liquids*, Academic Press, 3rd edn, 2006.

57 B. W. Russel, D. A. Saville and R. W. Schowater, *Colloidal Dispersions*, Cambridge University Press, 1989.

58 R. M. Fuoss and H. Sadek, *Science*, 1949, **110**, 552.

59 A. Michaels and R. Miekka, *J. Phys. Chem.*, 1961, **65**, 1765.

60 A. V. Dobrynin and M. Rubinstein, *Prog. Polym. Sci.*, 2005, **30**, 1049.

61 C. Meng and A. Rudin, *Makromol. Chem., Rapid Commun.*, 1981, **2**, 655.

62 A. Dondos, *J. Polym. Sci., Part B: Polym. Phys.*, 2006, **44**, 1106–1112.

63 P. J. Flory, *Principles of polymer chemistry*, Cornell University Press, Ithaca, New York, 1953, p. 611.

64 H. Dautzenberg and G. Rother, *Macromol. Chem. Phys.*, 2004, **205**, 114.

65 H. Dautzenberg, *Macromolecules*, 1997, **30**, 7810.